Received: 27 May 2020 | Revised: 10 October 2020 | Accepted: 17 November 2020

IET Microwaves, Antennas & Propagation

DOI: 10.1049/mia2.12084

The Institution of Engineering and Technology WILEY

ORIGINAL RESEARCH PAPER

Compact beam-switchable antenna for mm-wave 5G handheld devices

Farzana Arshad[1] | **Zia Ullah Khan**[2] | **Ahsan Ali**[3] | **Yasar Amin**[1] | **Hannu Tenhunen**[4,5]

[1]Telecommunication Engineering Department, University of Engineering & Technology Taxila, Pakistan

[2]School of Electronic Engineering and Computer Science, Queen Mary University of London, London, UK

[3]Department of Electrical Engineering, University of Engineering & Technology Taxila, Pakistan

[4]Department of Electronic Systems, Royal Institute of Technology (KTH), Stockholm, Sweden

[5]Department of Information Technology, TUCS, University of Turku, Turku, Finland

Correspondence

Farzana Arshad, Telecommunication Engineering Department, University of Engineering & Technology Taxila, 47050, Pakistan.
Email: farzana.arshad@uettaxila.edu.pk

Abstract

An electronically beam-steerable antenna (BSA) is envisioned. The presented BSA is a possible solution to overthrow the limitations inherent to phased antenna arrays. The design consists of a gap coupling inset feed rectangular patch (driven element) and 3 × 1 passive parasitic patches deployed on both sides of the driven patch. Prototype having 20 × 20 mm dimensions is printed on Rogers® RT/duroid®5870. Four switches are used to load the reactive impedance on parasitic patches, which in turn, change the phases of surface current on parasitic elements and the driven element. Based on the different ON and OFF configuration of switches in parasitic array elements, the main beam is steered along with different directions. The simulated results show that the design can operate between 26.8 and 30.3 GHz a wide impedance bandwidth $|S_{11}| < -10$ dB (12.5%) with a peak gain of 8.9 dBi and wide 3-dB scanning angle that is, −37° to 156° in the azimuth plane. The exhibited performance of BSA with favourable characteristics, such as wideband, adequate gain, wide-angle beam switching, and low profile renders the BSA a good candidate for 5G millimetre wave handheld devices. Moreover, to corroborate the performance, the design is fabricated, and experimental measurements were performed. Congruence is observed between the experimentally measured and computationally simulated results. The simulated results of spherical coverage analysis of BSA with the integration of smartphone form factor are also presented.

1 | INTRODUCTION

Fifth-generation communication (5G) is an emerging technology aimed at addressing the staggering growth in demand for capacity and data rate by utilizing the band of millimetre wave (MMW) spectrum. MMW frequencies for the first time are adapted for mobile phone communication, and it is proclaimed that 5G will be commercialized in 2020. The frequencies in the MMW band remain susceptible to high transmission path losses, but the available bandwidth is far higher than that offered by the microwave band [1–3], enabling broadband mobile communication. Base stations and user equipment need to be equipped with high-gain or beam-steerable arrays to vanquish the path loss over the millimetre wave band of operation. The high gain antenna arrays have narrow half-power beam width (HPBW) hence coverage is small. The most common way to realize a steerable array is to implement the phased array using a hybrid approach combining analogue phase shifters and digital beamforming techniques [4]. However, due to prevalent physical space constraints at the user terminal, the deployment of the phased array remains a long-standing challenge.

In the recent past, attempts at designing beam steerable array for mobile devices at millimetre wave frequencies have been made wherein different phased arrays have been proposed [5–9]. In [5], a planner switchable 3D coverage phased array with 2 GHz bandwidth and with maximum coverage efficiency of 74.3% is presented. Electronically beams are switched in three distinct regions utilizing the three phased arrays.

In [6], three sub-arrays were employed; each array consists of eight patch elements with the ability to steer the beams in 0° to 75° with 1 GHz bandwidth. Four sub-arrays capable of steering the beams up to 90° with 4 GHz bandwidth have been discussed in [7]. A Radio Frequency Identification Circuit (RFIC) for implementation of progressive phase shift is utilized, paving the way for array scanning. In [8], the scanning range from 0° to 60° is achieved using two-phased arrays. Each phased array is

realized using eight phase shifters. The impedance bandwidth of the proposed design is 2.5 GHz. In [9] 2 × 2 and 3 × 3 series-fed phased antenna array has been demonstrated to acquire the scanning range of up to ±25° and ±20°, respectively. The 0.7 and 1.6 GHz bandwidth is reported for two designs. A beam-steerable phased array based on the Quasi-Yagi antenna array having 2 GHz bandwidth was proposed in [10]. The proposed design can scan from 0° to 75°. The coverage efficiency of above-mentioned designs is not demonstrated. Despite good coverage and steering capability offered by phased arrays, certain drawbacks including large space occupied by phase shifters and complexity of hardware implementation require a thorough address. Moreover, phased arrays with analogue phase shifters lead to high losses at millimetre wave frequency. Consequently, digital beamforming requiring complex signal processing and large power consumption become quite expensive, deterring mass adaption of the technique for consumer-centric products [4, 11, 12]. Also, the incorporation of multiple sub-arrays within a single device remains a long-standing challenge.

In [13], two elements-based MIMO system has been proposed. Each element contains 4 × 4 antennas. It's capable of steering the beam only in 150° and 135° direction. In [14], two arrays having four elements based on the Quasi-Yagi antenna envisioned using a 10-layer PCB stack configuration. Both arrays have been mounted on different sides of a mobile chassis capable of steering the beam at 30° and 42°. In [15], a substrate integrated waveguide (SIW) based multi-beam slot array has been proposed. Multi-beams are achieved through a butler matrix. This design forms the beams at ±13° and ±51° with four different ports. A 16-elements planar array capable of beam switching at ±42° is proposed in [16]. The designs, as mentioned above, have an intricate geometrical structure. Most constituent beamforming networks in the designs, as mentioned earlier, also require an inconveniently sizeable physical footprint. Designs that are affordable in terms of fabrication cost and low in the profile are direly needed for real-world use and extensive applications. Furthermore, while the realization of low-profile, low-cost multilayer, beamforming networks is possible through substrate integrated lens, the technique presents high losses as reported in [17, 18].

Extensive research has been carried out on an electronically steerable passive array radiator [19–23]. In this technique, different reactive impedances are loaded on parasitic elements, which change the phases of surface current density on parasitic elements and the driven element. As an outcome of difference in phase, array-based designs allow the beam to be steered in different directions by using a single driven element. However, previous work based on this technique [19–23] has been focussed on lower frequencies and does not accommodate for mobile terminals.

Two identical reconfigurable radiating elements (RRE) are connected through an electromechanical radio frequency switch. Both RRE can steer the beam (one in +direction, other in −direction) to 0°, ±30° and ±45° directions at the cost of a very complicated structure [24]. In [25], the design comprises of three monopoles. One of the monopole antennas is directly fed through SIW whereas the other two monopoles act as parasitic elements. Two reflective switches, each having 1-input and 4-output (1P4T), are implemented. Eight short-circuited transmission lines are used and connected with four outputs of each switch. With this configuration, scanning angle ≥90°, a bandwidth of 2 GHz and a maximum gain equal to 9.3 dBi is achieved. In [26], the architecture consists of a Quasi-Yagi antenna array able to cover an area of 180°. The overall size of this design is 130 mm × 70 mm × 0.762 mm. The average gain has been reported to be 8 dBi. Coverage efficiency is also demonstrated in [25, 26].

The objective of this paper is to propose a simple, compact, low-cost beam-steerable structure for 28 GHz frequency. Compact size and low-cost features enable its suitability for mass-adoption and easy integration with 5G smart devices. The novelty of the beam-steerable antenna (BSA) is the realization of wide-area coverage with adequate gain and bandwidth with the most straight forward and compact structure.

The proposed design demonstrates the scanning range from −37° to 156°. A simple switching technique is employed to steer the beam and scan the different portions of space without using traditional means of realizing phase shifters. Owing to compact size, the antenna can be deployed on the top portion of the chassis of mobile device the area which is not commonly covered by the user's hand while placing a call. Inadvertently 5G mm-Wave radio signals are prevented from coming through by human hand, head or nose as these signals are sensitive to blockage [27].

2 | WORKING PRINCIPLE OF PROPOSED DESIGN

Yagi-Uda principle can be used to describe the operational mechanism of the proposed design, where parasitic elements are coupled through energy radiated by the driven dipole; consequently, a directional beam is formed [28]. In [29], a microstrip Yagi antenna is proposed to tilt the main beam with the help of parasitic elements placed on the same plane. If the length of the parasitic patch is slightly longer than the driven element, it acts as a reflector. On the other hand, it functions as a director if the length of the parasitic element is shorter [30]. Capacitive and inductive effects are introduced when parasitic elements act as directors or reflectors, respectively. Consequently, the phases of the surface current densities on both types of elements change correspondingly. This change in phase causes the main beam to steer away from the broadside direction.

In the proposed design, the mutual coupling takes place between the driven element and two 3 × 1 square-shaped reconfigurable array elements. Varying the ON and OFF state of interconnected switches the effective electrical length of the constituent array elements can be changed. This configuration allows the array elements to act as a reflector or director steering the beam in different directions.

3 | DESIGN CONFIGURATION

Figure 1 depicts the geometry and configuration of the BSA. Initially, a gap coupling inset feed rectangular patch (driven

element) is designed to operate at 28 GHz. Gap coupling inset feed is designed to enhance the −10 dB impedance bandwidth. Geared towards achieving the beam steering, the parasitic coupling is introduced by longitudinally deploying the 3 × 1 square-shaped parasitic patches on the left and right side of the driven element. Four switches are used to make a connection between the parasitic elements. Rogers® RT/duroid®5870 ($\varepsilon r = 3.33$, $\tan\delta = 0.0009$, $h = 0.8$ mm) backed with copper ground is used as a substrate.

The size of the BSA is 20 × 20 mm. The already published equations are used to compute the dimensions of the patch [31].

Simulation and optimization are carried out using CST® Microwave Studio®. Multiple prototypes are fabricated to validate the electromagnetic performance of the realized BSA. A rectangular patch antenna with gap-coupled inset feed is designed to operate at 28 GHz frequency. Forging ahead, two passive arrays consisting of 3 × 1 square patches are formulated. The length of the passive elements is 30% less than that of the driven element to ensure the maximum coupling. It is also observed that if the length of parasitic elements is reduced below the optimized value, sidelobe levels drastically increases and the peak gain is reduced.

The connection between parasitic elements is made via diodes. Four switches, *S*1, *S*2, *S*3 and *S*4 have been configured, as shown in Figure 1. Considering six different ON and OFF combinations of switches (as detailed in table [1]), significant changes in radiation pattern are observed. In Table 1, '0' indicates the disconnected state, that is, OFF status of a switch, whereas '1' signifies the connected state, that is, ON status of a switch. The gap between the driven and parasitic elements is ≤0.5 λ, where λ is the operating wavelength of the proposed design. This gap has been chosen to reduce the sidelobe levels, also to ensure maximum coupling between the parasitic element and the driven one.

Four PIN diode MA4AGBL912 switches are used. These switches can work up to 40 GHz. The resistive, capacitive and inductive parameters of the switches have been adapted from the product datasheet. The detailing that the ON state of the PIN diode is corresponding to a series resistance $Rs = 4.2\ \Omega$, and an inductance $Ls = 0.5$ nH.

A series capacitance Ct equals to 28 fF, and an inductance is given by $Ls = 0.5$ nH is corresponding to the OFF state of the PIN diode. The equivalent diode model is illustrated in Figure 2.

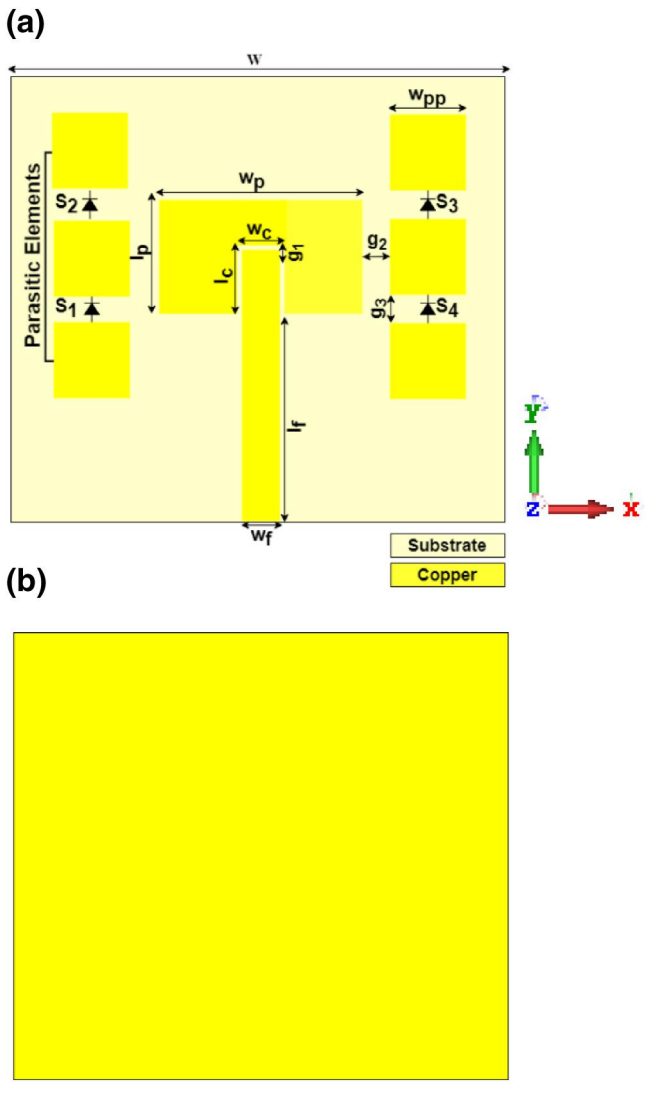

FIGURE 1 Geometry of BSA (a) front view (b) back view

4 | SIMULATED RESULTS AND DISCUSSION

4.1 | Parametric analysis

Different values for parameters g_2 and w_p, which is the gap between driven element and parasitic element and the length of

TABLE 1 Six different operating modes of BSA due to ON and OFF combination of switches

Modes	*S*1	*S*2	*S*3	*S*4	Scanning Angle
1	0	0	0	0	89
2	1	1	0	0	−37
3	1	1	0	1	10
4	0	0	1	1	156
5	0	1	1	1	117
6	1	0	1	1	137

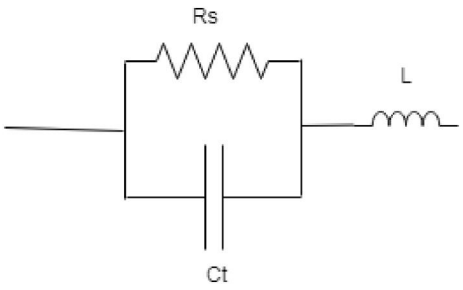

FIGURE 2 Diode model

TABLE 2 Dimensions of the proposed design (unit: mm)

W	w_p	l_c	w_f	l_f	l_p	w_{pp}	w_c
20	4.44	1.3	1.7	9.3	3.22	2	1.8
g_1	g_2	g_3	W_2	L			
0.2	0.5	0.79	72	152			

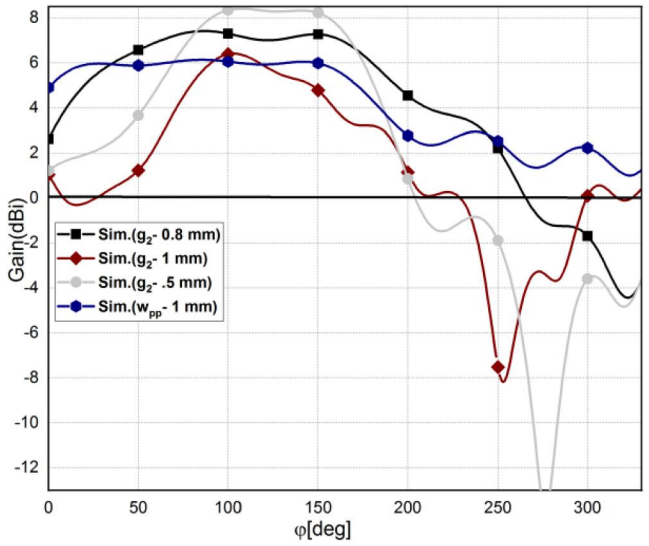

FIGURE 3 Parametric analysis of proposed BSA

parasitic elements, respectively, are chosen other than the optimized values as given in Table 2 to see their impact on the radiation pattern. If the gap between the driven element and parasitic elements is increased than the optimized value, it is observed that the gain, sidelobe levels decreases and beam width increases as compared to optimized values. If the length of the parasitic patches is less than the optimized value, the sidelobe levels drastically increase. The difference can be seen in Figure 3.

4.2 | Simulated results for optimized parametric values

Owing to the incorporation of parasitic elements and switches, not only does the main beam steer in different directions with each varying mode of operation but the impedance bandwidth also undergoes a corresponding change. Figure 4 illustrates the simulated *S*-parameters of the proposed design in different operating modes. With the specification of −10 dB, the obtained impedance bandwidth of the driven element is from 26.8 to 30.3 GHz. In Mode 1, when all switches exhibit an OFF state, the *S*-parameter enhanced and undergoes a slight shift towards the right. In other ON and OFF combinations of switches, the *S*-parameter exhibits a change in each state. It is observed that the impedance bandwidth gets wide, and central frequency is drifted during different operating modes due to parasitic elements and reactive impedance loading, still even then, the central frequency remains well within the impedance

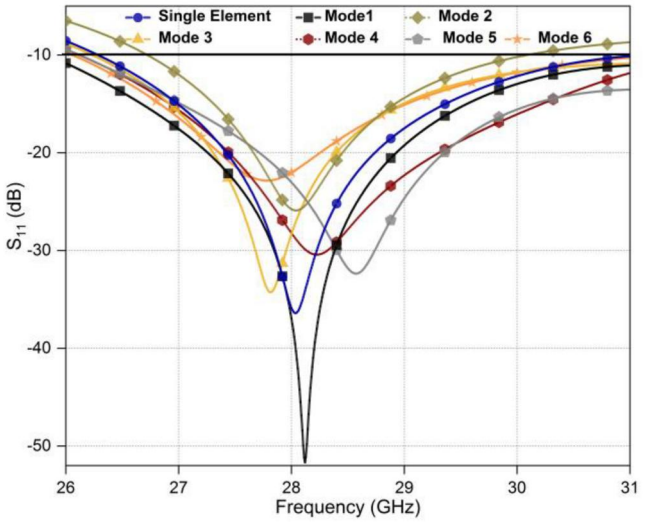

FIGURE 4 *S*-parameter of proposed BSA in different modes

bandwidth corresponding to a single element. Across all six operating modes, the common impedance bandwidth ranges from 26.8 to 30.3 GHz.

Figure 5 shows the simulated 3D radiation pattern of the proposed beam-steerable design at 28 GHz. From Figure 4, it can be observed that with six different operating modes, the antenna is capable of steering the beam at −37°,10°,89°,117°,137° and 156°, respectively. In Mode 1, when all switches are OFF the beam is directed towards 89°, whereas, in Mode 2, when all left switches are ON, the beam shifts towards −37°. In Mode 4, when only right switches are on, the beam is directed towards 156°. Intermediate beam switching is obtained due to ON and OFF combination of left- and right-side switches, as depicted in Table 1. The asymmetrical result of beam steering is obtained due to different spacing between the left side, right side parasitic elements and the driven element. It is observed that if the distance between both side parasitic elements, and driven element kept the same the gain drops.

The scanning property of the proposed design can be better analysed through 2D-radiation, as shown in Figure 6. Figure depicts that the overall scan coverage range goes up to 280° with a peak gain of 8.9 dBi. According to half-power beamwidth (HPBW) Mode 4 can scan from 210° to 80°, and Mode 2 can scan from −70° to 55°. All other modes can scan between these two limits. Hence the total spherical coverage is 280° covered by all operating modes of BSA. All modes have wide HPBW hence can scan the large area.

In Mode 1, 8.9 dBi peak gain is observed when all switches are OFF. In Mode 2 and Mode 3, 8.46 dBi and 8.89 dBi peak gain is demonstrated at −37° and at 10°. The peak gain of 8.66, 8.45 and 8.56 dBi is observed at 156°, 137° and 117°, respectively for Mode 4, Mode 5 and Mode 6. Except for Mode 1, where all switches are OFF, the gain is reduced in all other modes from 8.9 dBi because of lossy switches. Maximum peak gain is observed in Mode 1 when all switches are in the OFF state.

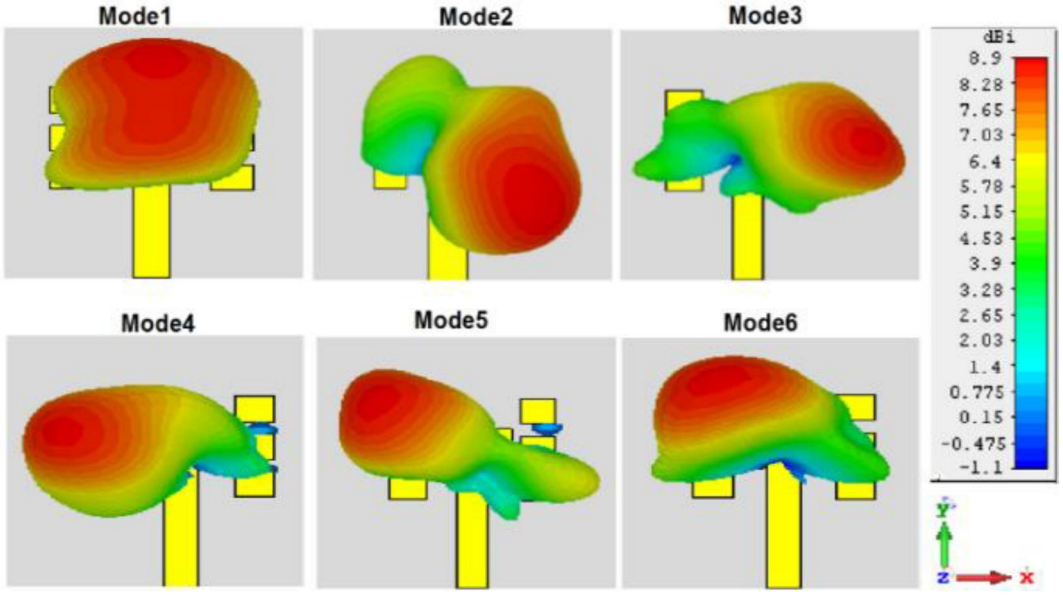

FIGURE 5 Simulated 3D radiation pattern in different operating modes

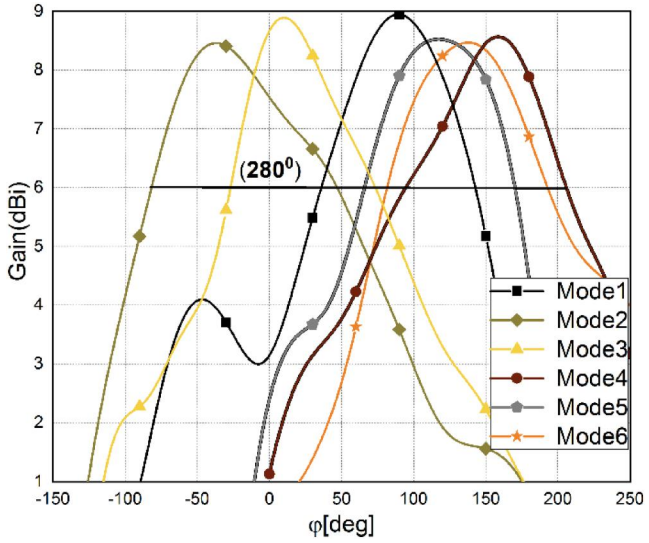

FIGURE 6 Spherical coverage of proposed BSA

5 | EXPERIMENTAL AND NUMERICAL RESULTS

The proposed BSA is fabricated and measured for validating the performance parameters. Figure 7a-c illustrates the prototypes of the antenna in different operating modes. Measurements are taken for three different operating modes (Mode 1, Mode 2 and Mode 4) of the proposed design, demonstrating the optimal results in terms of gain and beam-switching. Maximum gain is observed in Mode 1, that is when all switches are OFF. Mode 2 and Mode 4 correspond to maximum beam switching capability of the proposed design in both the left and right directions. Prototypes are used to validate the simulated results instead of presenting the final realistic scenario. Actual switches are not used in fabricated design as it remains extremely challenging to control the accuracy when soldering the switches between such minuscule array elements which have been separated by a distance of less than 1 mm. Simply the parasitic elements are shorted out.

PNA-X Network Analyzer (Keysight Technologies N5244A) is utilized to measure the *S*-parameter of the fabricated prototypes. The comparison of simulated and measured *S*-parameter is illustrated in Figure 8. It is observed that the measured *S*-parameter undergoes a shift. A significant drift is observable in the case of Mode 2 and Mode 4. The values, however, remain between the required bands. The common simulated impedance bandwidth (<−10 dB) among all modes extends from 26.8 to 30.3 GHz. The shared measured impedance bandwidth (<−10 dB) between all three modes ranges from 27 to 29.2 GHz. The fabrication limitations posed by a milling machine, substrate permittivity variations at higher frequencies, and shortening of patches caused the slight difference that exists between measured and simulated results.

The radiation pattern is measured utilizing the NSI-MI planar near-field beam pattern scanner. Figure 9 depicts the Radiation pattern measurement setup. Fourier transform algorithm is applied to convert the measured radiating energy in the near-field region to far-field results [32].

Figure 10 depicts the H- plane simulated and measured radiation patterns at 28 GHz for different three operating modes of the proposed design. In particular, the radiation pattern is measured for φ values ranges from 0° to 180° and 0° to −180°. It can be seen that the scanning angle in these three measured states is slightly different from simulated states, which is due to fabrication-related inaccuracies. It is also observed that the beamwidth of the experimentally measured

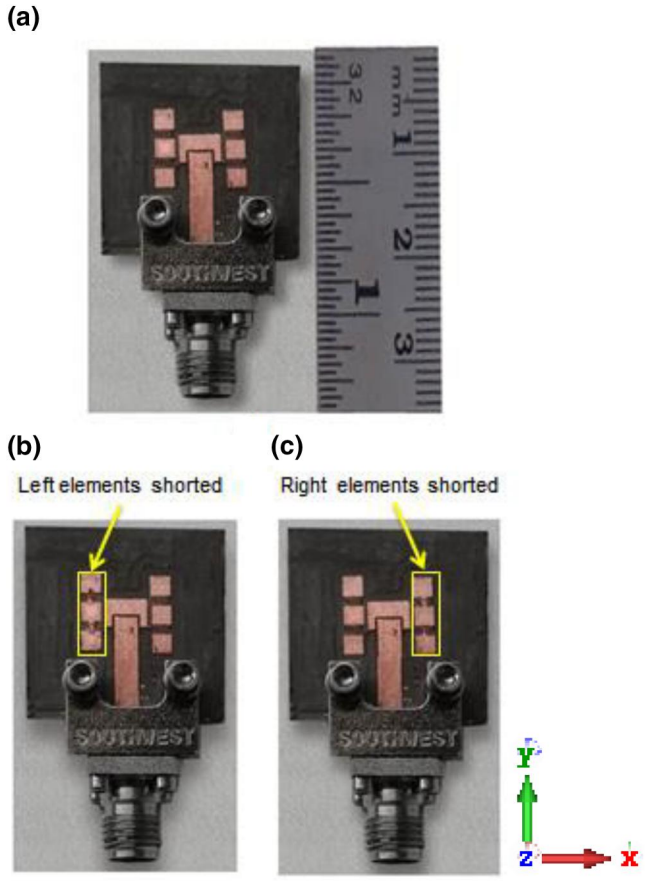

FIGURE 7 Fabricated prototypes of proposed design: (a) parasitic elements are not shorted (b) Right-sided short patches (c) Left-sided short patches

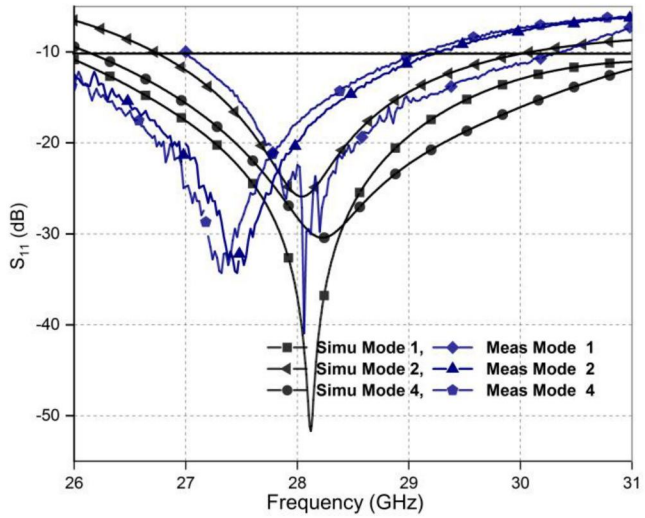

FIGURE 8 Comparison of simulated and measured *S*-parameters

radiation pattern in each mode is larger than the simulated results.

Table 3 presents the simulated and measured realized gain of the proposed prototype against the frequencies and

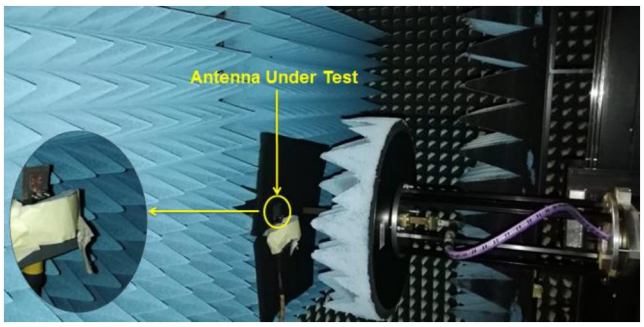

FIGURE 9 Measurement setup

operating modes. The gain comparison method is used [31] for measured gain. The measured characteristics of the antenna under test (AUT) are compared with that of the standard horn antenna to measure the gain of AUT. The maximum gain is 8.88 dBi, which is in good agreement with the simulated gain at 28 GHz in Mode 1.

6 | IMPACT OF PIN-DIODES AND OPEN/SHORT CIRCUIT ON RADIATION EFFICIENCY AND IMPEDANCE MATCHING

The simulated radiation efficiency and impedance matching of BSA in different configurations are presented in Figures 11 and 12, respectively. Figure 11 shows the comparison of impedance matching when parasitic elements are connected through PIN-diodes and when the parasitic elements are simply shorted/opened. It is observed that when the circuit is short/open the frequency band shifted towards the left side but covers the required operating band. It is also observed impedance matching enhanced in case of short circuit.

The proposed antenna array exhibits high radiation efficiency (>90%). It can be observed from the figure that when switches are ON/OFF the radiation efficiency is slightly lower than the case of open and short-circuited. The maximum radiation efficiency is observed in the case of the short circuit.

7 | THE SPHERICAL COVERAGE ANALYSIS OF BSA WITH THE INTEGRATION OF SMARTPHONE FORM FACTOR

The spherical coverage is known as the range of solid angles to be covered by a user terminal. In the mobile communications, the orientation of user terminal and angle of incoming signals are random. Hence spherical coverage analysis is import for the user terminal. Owing to the sparser nature of the channel at mm-wave the spherical coverage is going to be a critical parameter. For spherical coverage analysis, the parameters like coverage efficiency and total scan pattern have been used [5, 6, 25, 26, 33]. In literature the coverage is evaluated by coverage efficiency in

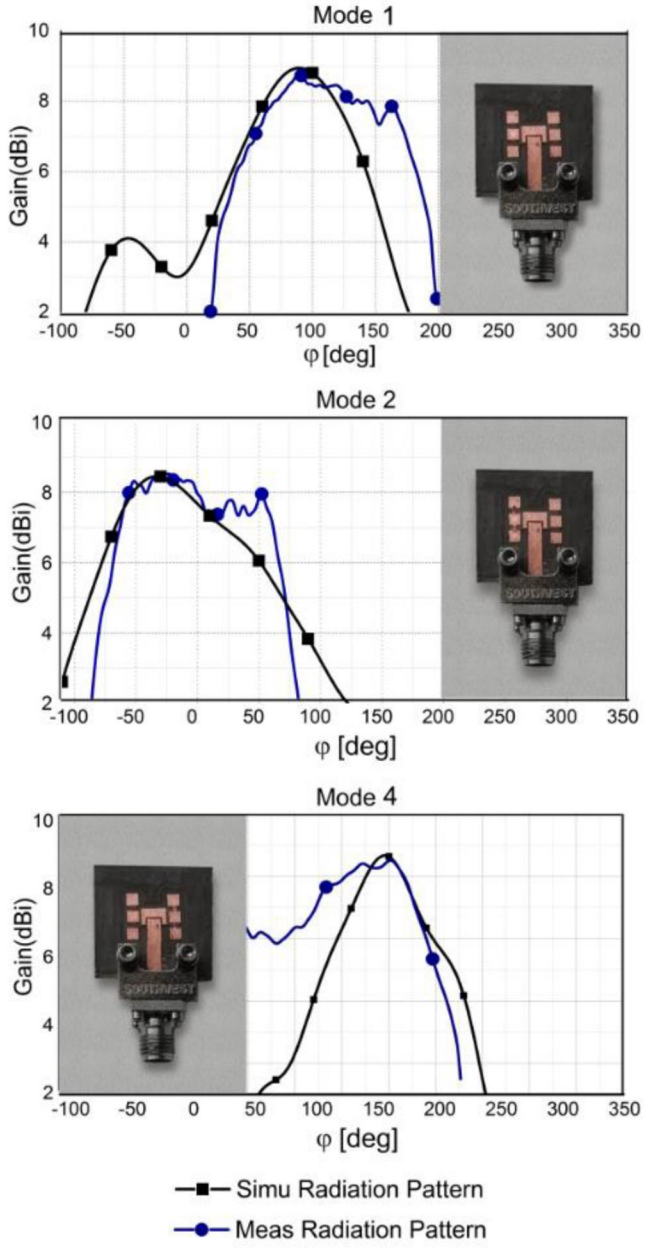

FIGURE 10 Simulated and measured radiation pattern (a) Mode 1 (b) Mode 2 (c) Mode 4

TABLE 3 Comparison simulated and measured gain in three different modes of BSA

		Peak Gain (dBi)	
Frequency (GHz)	**Mode**	**Simulated**	**Measured**
28	1	8.9	8.88
28	2	8.46	7.99
28	4	8.66	8.1

terms of gain. In wireless communication, other parameters like the transmitted power/receive sensitivity and the transmission losses in the radio frequency (RF) chain are also important along with antenna gain to analyse the spherical coverage of user

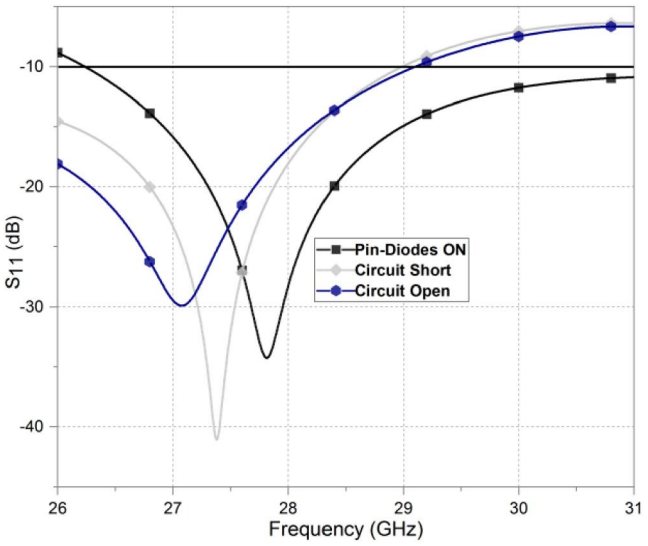

FIGURE 11 Comparison of impedance matching with PIN diodes and with open and short circuit

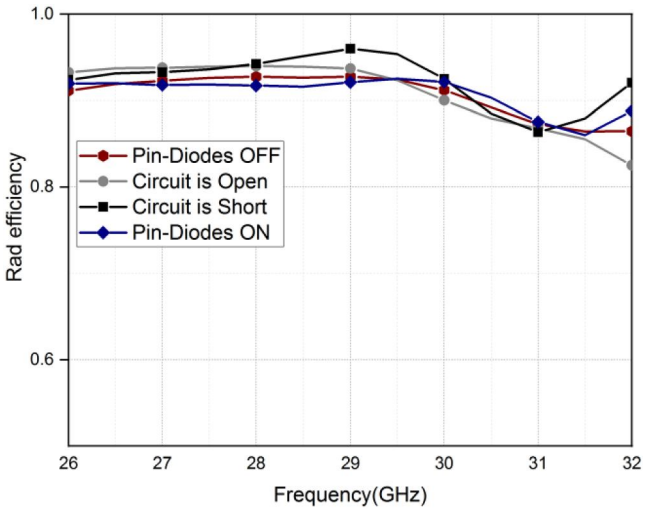

FIGURE 12 Comparison of rad efficiency with PIN diodes and with open and short circuit

terminal. In [34] according to 3GPP specification release (15), the uplink spherical coverage of a user terminal is specified by cumulative distribution function (CDF) of EIRP for frequency range 2. The measure of power in specific direction along with transmitted power and the transmission loss in the RF chain and antenna gain is known as EIRP. Equation (1) is used to calculate the CDF of user terminal's EIRP.

$$\mathrm{CDF(EIRP)} = P(\mathrm{EIR_{PUT}}(\theta, \phi) < \mathrm{EIRP}) \qquad (1)$$

where P is probability function density of EIRP.

Figure 13 shows the form factor of a smartphone which is designed based on the information given in [34-36] The material used in the back cover is plastic having a permittivity of 2.7 and the loss tangent around 0.004. The front panel is

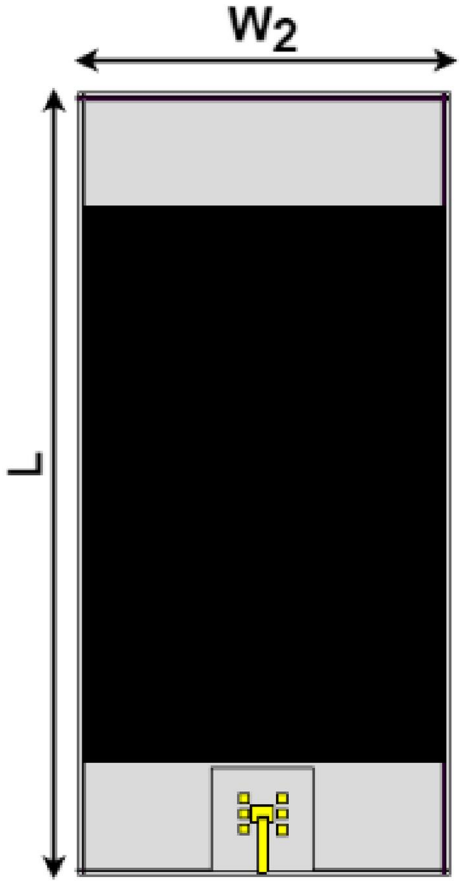

FIGURE 13 Configuration of BSA with smartphone form factor

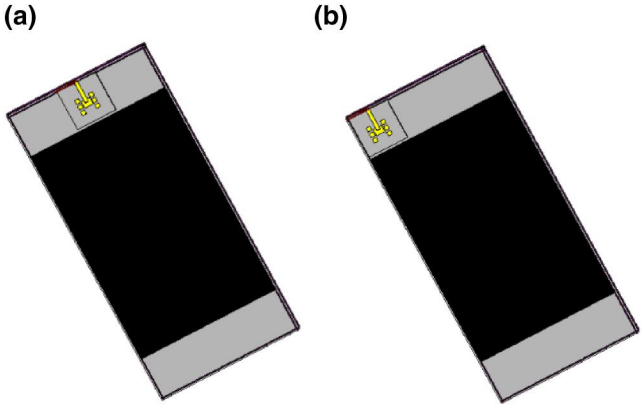

FIGURE 14 Simulation model of BSA configuration in mobile device with smartphone factor (a) Configuration 1 (b) Configuration 2

composed of gorilla glass. The other electronic components inside the mobile are considered as a metal.

To observe the impact on the spherical coverage from the placement of BSA, two configurations of BSA with smartphone factor are considered as shown in Figure 14. The BSA is kept on the front side of the device in both configurations. The CDF of EIRP is calculated based on these two configurations. The simulated CDF of EIRP is presented in Figure 15. In simulations, 12 dBm accepted power into antenna port is considered to normalize the EIRP value which is 22.4 dBm according to 3GPP specifications at 28 GHz. It can be observed from the figure that the peak value of EIRP in both cases is similar. However, the EIRP value at CDF = 50% is different in both configurations. In Configuration 1, EIRP at CDF = 50% is around 10 dBm, and in Configuration 2 EIRP at CDF = 50% is around 12.5 dBm. According to the 3GPP specification, the user terminal minimum EIRP at CDF = 50% should be 11.5 dBm and minimum peak EIRP will be 22.4 dBm. From the figure of CDF of EIRP, it can be observed that the peak EIRP is closer to the peak EIRP values given in the 3GPP specifications. In Configuration 2, EIRP at CDF = 50% met the 3GPP required values.

8 | COMPARISON WITH STATE-OF-THE-ART

The performance of the proposed design is compared with recent work reported in the literature focussed on BSAs for 5G handheld devices.

In [26], two identical radiating reconfigurable structures (RRS) are connected through an electromagnetic radio switch. RRS is based on the rectangular waveguide. A reconfigurable semiconductor circuit (RSC) is placed inside the waveguide. RSC has 15 reconfigurable slots with embedded S-PIN diodes. Only five beams are formed with this complex structure with a maximum of 6 dBi gain. The design proposed in [27], consists of three monopoles. A driven monopole is directly fed by SIW and two parasitic monopoles. A pair of 1-input and 4-output (1P4T) reflective switches are implemented. For every switch, each of the four outputs is connected with four short-circuited transmission lines. With this configuration, scanning angle ≥90°, the bandwidth of 2 GHz and a maximum gain equal to 9.3 dBi are achieved. In [28], architecture consists of a Quasi-Yagi antenna array able to cover an area of 180°. The overall size of this design is 130 × 70 ×0.762 mm. The proposed design occupies 2 × 2 × 0.8 mm area and provides sectoral coverage of 280° because of broad beamwidth of radiation pattern and switching capability in different directions with adequate bandwidth and gain (Table 4).

9 | CONCLUSION

A BSA for 28 GHz band based on the parasitic coupling is demonstrated The design consists of a gap coupled inset feed rectangular patch antenna, and two 3 × 1 parasitic square-shaped patches realized on both sides of the driven element. Parasitic elements are interconnected with four PIN diodes. Based on the ON/OFF states of the switches, six beam-steering is generated with wide 3-dB beamwidth, which offers the spherical coverage of 280° with a maximum and minimum gain of 8.9 dBi and 8.45 dBi, respectively. The BSA is able to steer the beams from −37° to 156° and is implemented with minimal hardware complexities. The proposed design is prototyped, and measurements are made for validating this

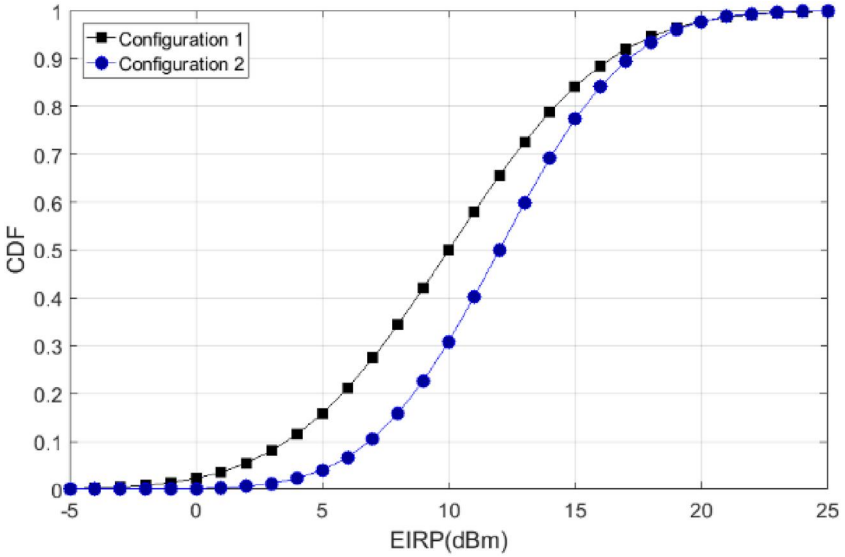

FIGURE 15 CDF of EIRP of proposed BSA in two different configurations

TABLE 4 Comparison with state-of-the-art

Ref	No. of Switches	Beam Steering Range	Realized Gain (dBi)	Frequency BW (GHz)	Size (mm)	Structure
[27]	1Electromechanical radio frequency switch 15 S-PIN diodes	−45 to +45	6.5	2%	276 × 40	Complex (two port)
[28]	2 reflective switches (1 input 4 output of each switch)	60° to 180°	9.3	15%	65 × 30	SIW
[29]	Four-throw (SP4T) switches	−19° to −147°	8	Multiband 19%	130 × 70	Quasi-Yagi array
This work	4 PIN diodes	−37° to 156°	8.96	10.7%	20 × 20	Simple patch

alternative approach. The measured results are in accordance with the simulated results, which prove the suitability of the design for 5G beam steerable handheld devices. Due to minuscule footprint, this structure can be positioned on top of a mobile device to minimize the signal blockage by hand or fingers of user.

ACKNOWLEDGEMENTS

The authors would like to thank the Queen Mary University of London (QMUL), for the design fabrication and testing services.

ORCID

Ahsan Ali https://orcid.org/0000-0002-3583-393X

REFERENCES

1. Cano, R.R., et al.: Reduction of main beam-blockage in an integrated 5G array with a metal-frame antenna. IEEE Trans. Antennas Propag. 67(5), 3161–3170 (2019)
2. Shakib, S., et al.: mmWave CMOS power amplifiers for 5G cellular communication. IEEE Commun. Mag. 57(1), 98–105 (2019)
3. Nguyen, T.Q.K., et al.: Experimental evaluation of user's finger effects on a 5G terminal antenna array at 26 GHz. IEEE Antennas Wirel. Propag. Lett., 1–1 (2020)
4. Naqvi, A.H., Lim, S.: Review of recent phased arrays for millimetre-wave wireless communication. Sensors. 18(10), 3194 (2018)
5. Zhang, S., et al.: A planar switchable 3-D-coverage phased array antenna and its user effects for 28-GHz mobile terminal applications. IEEE Trans. Antennas Propag. 65(12), 6413–6421 (2017)
6. Ojaroudiparchin, N., et al.: A switchable 3-D-coverage-phased array antenna package for 5G mobile terminals. IEEE Antennas Wirel. Propag. Lett. 15, 1747–1750 (2016)
7. Stanley, M., Huang, Y., Wang, H.: A capacitive coupled patch antenna array with high gain and wide coverage for 5G smartphone applications. IEEE Access. 6, 41942–41954 (2018)
8. Yu, B., et al.: A novel 28 GHz beam steering array for 5G mobile device with metallic casing application. IEEE Trans. Antennas Propag. 66(1), 462–466 (2018)
9. Khalily, M., et al.: Design of phased arrays of series-fed patch antennas with reduced number of the controllers for 28-GHz mm-wave applications. IEEE Antennas Wirel. Propag. Lett. 15, 1305–1308 (2016)
10. Prachin, N.O., Alibakhshikinari, M., Basherlou, H.J.: MM-wave phased array quasi-yagi antenna for the upcoming 5G cellular communications. Appl. Sci, 9(5), pp. 978 (2019)
11. Alkhateeb, A., MO, J., Gonzalez, P.N, et al.: MIMO precoding and combining solutions for millimetre-wave systems. IEEE Commun. Mag. 52(12), 122–131 (2014)
12. Ilram, M., et al.: A switched beam millimeter wave array with MIMO configuration for 5G applications. Microw. Opt. Technol. Lett. 60(4), 915–920 (2018)

13. Hwang, I., et al.: Quasi-Yagi antenna array with modified folded dipole driver for mmWave 5G cellular devices. IEEE Antennas Wirel. Propag. Lett. 18(5), 971–975 (2019)
14. Yang, Q., et al.: SIW multibeam array for 5G mobile devices. IEEE Access. 4, 2788–2796 (2016)
15. Klionovski, K., Sharawi, M. S., Shamim, A.: A dual-polarization-switched beam patch antenna array for millimeter-wave applications. IEEE Trans. Antennas Propag. 67(5), 3510–3515 (2019)
16. Lian, J.W., et al.: SIW folded cassegrain lens for millimeter-wave multi-beam application. IEEE Antennas Wirel. Propag. Lett. 17(4), 583–586 (2018)
17. Zhang, Y.S., Hong, W.: A millimeter-wave gain enhanced multibeam antenna based on a coplanar cylindrical dielectric lens. IEEE Trans. Antennas Propag. 60(7), 3485–3488 (2012)
18. Ouyang, W., Gong, X.: An electronically steerable parasitic array radiator (ESPAR) using cavity-backed slot antennas. IEEE Antennas Wirel. Propag. Lett. 18(4), 757–761 (2019)
19. Zhang, S., et al.: A planar switchable 3-D-coverage phased array antenna and its user effects for 28-GHz mobile terminal applications. IEEE Trans. Antennas Propag. 65(12), 6413–6421 (2017)
20. Towfiq, M.A., et al.: A reconfigurable antenna with beam steering and beamwidth variability for wireless communications. IEEE Trans. Antennas Propag. 66(10), 5052–5063 (2018)
21. Yang, Y., Zhu, X.: A wideband reconfigurable antenna with 360° beam steering for 802.11ac WLAN applications. IEEE Trans. Antennas Propag. 66(2), 600–608 (2018)
22. Hossain, M.A., Bahceci, I., Cetiner, B.A.: Parasitic layer-based radiation pattern reconfigurable antenna for 5G communications. IEEE Trans. Antennas. Propag. 65(12), 6444–6452 (2017)
23. Li, Z., et al.: A new class of antenna array with a reconfigurable element factor. IEEE Trans. Antennas Propag. 61(4), 1947–1955 (2013)
24. Yashchyshyn, Y., et al.: 28 GHz switched-beam antenna based on S-PIN diodes for 5G mobile communications. IEEE Antennas Wirel. Propag. Lett. 17(2), 225–228 (2018)
25. Zhang, S., Syrytsin, I., Pedersen, G.F.: Compact beam-steerable antenna array with two passive parasitic elements for 5G mobile terminals at 28 GHz. IEEE Trans. Antennas Propag. 66(10), 5193–5203 (2018)
26. Paola, C.Di., Zhang, S., Zhao, K.: Wideband beam-switchable 28 GHz quasi-yagi array for mobile devices. IEEE Trans. Antennas Propag. 67(11), 6870–6882 (2019)
27. https://www.eetimes.com/mwc-are-your-5-fingers-blocking-your-5g/ Accessed 5 April 2020
28. https://www.electronics-notes.com/articles/antennas-ropagation/yagi-uda-antenna-aerial/theory.php/Accessed 5 March 2018
29. Huang, J.: Planar microstrip yagi array antenna. Antennas and Propagation Society International Symposium, AP-S. Digest. IEEE, pp. 894–897. (1989)
30. Huang, J., Densmore, A.C.: Microstrip yagi array antenna for mobile satellite vehicle application. IEEE Trans. Antennas Propag. 39(7), 1024–1030 (1991)
31. Balanis, C.A.: Microstrip Antennas in Antenna theory, 3rd ed, pp. 817–825.John Wiley and Sons, Hoboken, NJ, USA (2005)
32. NSI, MI. https://www.nsi-com/products/systemsolutions/near-field-systems. [Online]
33. Helander, J.: Millimeter Wave Imaging and Phased Array Antennas for 5G and Aerospace Applications. PhD thesis, Lund University (2019)
34. Zhao, K., et al.: Spherical coverage characterization of 5G millimetre wave user equipment with 3GPP specifications. IEEE Access. 7, 4442–4452 (2019)
35. Zhao, K., et al.: Body-insensitive multimode MIMO terminal antenna of double-ring structure. IEEE Trans. Antenn. Propag. 63, 1925–1936 (2015)
36. Raghavan, V., et al.: Statistical Blockage Modeling and Robustness of Beamforming in Millimeter-Wave Systems. IEEE Transactions on Microwave Theory and Techniques, 67(7), 3010–3024 (2019)

How to cite this article: Arshad F, Khan ZU, Ali A, Amin Y, Tenhunen H. Compact beam-switchable antenna for mm-wave 5G handheld devices. *IET Microw. Antennas Propag.* 2021;15:778–787. https://doi.org/10.1049/mia2.12084